

# Structure-Free Validation of Residual Dipolar Coupling and Paramagnetic Relaxation Enhancement Measurements of Disordered Proteins

Francisco N. Newby,<sup>†</sup> Alfonso De Simone,<sup>‡</sup> Maho Yagi-Utsumi,<sup>†,§</sup> Xavier Salvatella,<sup>^</sup> Christopher M. Dobson,<sup>†</sup> and Michele Vendruscolo<sup>\*,†</sup>

<sup>†</sup>Department of Chemistry, University of Cambridge, Cambridge CB2 1EW, U.K.

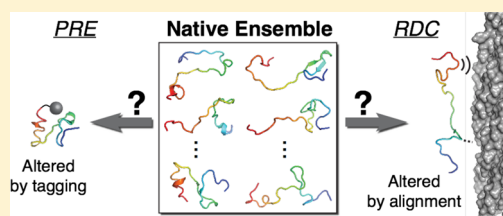
<sup>‡</sup>Department of Life Sciences, Imperial College London, South Kensington, London SW7 2AZ, U.K.

<sup>§</sup>Institute for Integrative Bioscience, National Institutes of Natural Sciences, 5-1 Higashiyama Myodaiji, Okazaki 444-8787, Japan

<sup>^</sup>ICREA and IRB Barcelona, Baldori Reixac 10, Barcelona 08028, Spain

## S Supporting Information

**ABSTRACT:** Residual dipolar couplings (RDCs) and paramagnetic relaxation enhancements (PREs) have emerged as valuable parameters for defining the structures and dynamics of disordered proteins by nuclear magnetic resonance (NMR) spectroscopy. Procedures for their measurement, however, may lead to conformational perturbations because of the presence of the alignment media necessary for recording RDCs, or of the paramagnetic groups that must be introduced for measuring PREs. We discuss here experimental methods for quantifying these effects by considering the case of the 40-residue isoform of the amyloid  $\beta$  peptide ( $A\beta_{40}$ ), which is associated with Alzheimer's disease. By conducting RDC measurements over a range of concentrations of certain alignment media, we show that perturbations arising from transient binding of  $A\beta_{40}$  can be characterized, allowing appropriate corrections to be made. In addition, by using NMR experiments sensitive to long-range interactions, we show that it is possible to identify relatively nonperturbing sites for attaching nitroxide radicals for PRE measurements. Thus, minimizing the conformational perturbations introduced by RDC and PRE measurements should facilitate their use for the rigorous determination of the conformational properties of disordered proteins.



Disordered states of proteins play crucial roles in the processes of protein folding and aggregation.<sup>1–5</sup> It is also increasingly clear that the presence of conformational disorder in native proteins is a widespread phenomenon of great significance, as intrinsically disordered proteins are closely involved in signaling and regulation, as well as in a range of medical conditions that include Alzheimer's and Parkinson's diseases.<sup>1–7</sup> Therefore, a better characterization of protein disorder at the molecular level could offer many opportunities to advance our understanding of fundamental aspects of molecular biology as well as for the development of effective therapies for currently incurable diseases.<sup>1–7</sup>

Disordered proteins rapidly interconvert between many structurally diverse conformations and are best described as conformational ensembles. Nuclear magnetic resonance (NMR) spectroscopy has proved to be uniquely able to capture these conformational fluctuations at high resolution and even enable the determination of disordered protein ensembles.<sup>8–16</sup> Two important observables that have grown in prominence for this purpose are residual dipolar couplings (RDCs) between pairs of nuclei in partially aligned protein samples<sup>13,14,17–19</sup> and paramagnetic relaxation enhancements (PREs), which exploit the enhanced dipolar relaxation of nuclear spins in the proximity of paramagnetic groups to obtain long-range distance information.<sup>9–11,20–24</sup> These observables

are particularly important as disordered proteins populate expanded conformations and yield few measurable short-range distances derived from nuclear Overhauser effects (NOEs), which are traditionally used to define the structures of ordered proteins by NMR spectroscopy.

As RDC- and PRE-based methods are becoming widespread for the study of disordered proteins, it is important to investigate the perturbations that their measurement can introduce, may bias subsequent analysis. As we will discuss, these perturbations are unlikely to be significant for folded proteins, and hence, their importance in the case of disordered proteins is just beginning to be recognized.

To measure RDCs, weak alignment of the protein molecules is induced by the presence of a liquid crystalline alignment medium,<sup>25,26</sup> which could alter the protein conformations through long-range interactions or even by direct binding to the surfaces of the alignment media (nematogens).<sup>27</sup> These perturbations could be expected to be more likely for disordered than for native proteins as their conformations are

Received: June 16, 2015

Revised: October 17, 2015

Published: October 19, 2015



not stabilized by large numbers of intramolecular contacts that are present in their ordered counterparts.

PRE measurements generally require tagging of the target protein with an extrinsic paramagnetic group, either through attachment of a chelating group that binds paramagnetic metal ions with high affinity or by direct conjugation of a stable nitroxide radical (commonly termed a “spin-label”). As such tags are typically at least 50% larger than naturally occurring amino acids, their presence may affect the structures and dynamics of proteins in the vicinity of the labeling site and even lead to the formation of non-native long-range interactions. Furthermore, additional problems may arise from a potential lack of specificity in labeling.

For ordered proteins, the effects of molecular alignment and paramagnetic tagging can in principle be determined by reference to known high-resolution structures of the protein of interest. However, in the case of disordered proteins, structural information is generally not available, and indeed, it is exactly for this purpose that RDCs or PREs are being measured in the first place. An alternative approach is to cross-validate the structures by showing that the different results obtained from subsets of RDC or PRE data are consistent with each other.<sup>12,28–31</sup> Such validation can, however, be challenging because of the large number of degrees of freedom of disordered proteins. Given these limitations, we describe in this paper approaches to permit structure-free validation of RDC and PRE measurements, which can allow them to be applied more rigorously in the study of disordered proteins, other biomolecules that exhibit large structural fluctuations, or indeed folded proteins whose structures are unknown.

## MATERIALS AND METHODS

**Preparation of A $\beta$ 40 NMR Samples.** Recombinant A $\beta$ 40 peptides with ammonium acetate counterions were obtained from AlexoTech (Umeå, Sweden) and handled on ice at all times. The peptide powder was solubilized in 10 mM NaOH at concentrations of 4–7 mg/mL and stored at –80 °C until required. To prepare NMR samples, A $\beta$ 40 stock solutions were diluted into sodium phosphate buffer (50 mM Na<sub>2</sub>HPO<sub>4</sub>/NaH<sub>2</sub>PO<sub>4</sub>) to give a final peptide concentration of 60–150  $\mu$ M. The final buffer consisted of 20 mM sodium phosphate, 0.5 mM EDTA, 0.02% (w/v) NaN<sub>3</sub> and contained 10% D<sub>2</sub>O. HCl was pre-added to the sodium phosphate to neutralize NaOH in the A $\beta$ 40 stock solutions, and if necessary, the samples were titrated to pH 7.4 by addition of 100 mM NaOH. Final sample volumes were 160–200  $\mu$ L and contained 10% D<sub>2</sub>O. All samples were ultracentrifuged for 20 min at 8500g to sediment any aggregates of peptide present before being transferred to 3 mm MATCH NMR tubes (Bruker BioSpin AG, Fällanden, Switzerland).

**Aligned Samples Containing Pf1.** Pf1 bacteriophage was obtained from Asla Biotech (Riga, Latvia). Buffer exchange was accomplished by precipitation in 1.25 M NaCl and ultracentrifugation for 1 h at 11300g and 30 °C. The pellet was washed three times with deionized water and resuspended in sodium phosphate buffer over 1–2 h at 4 °C. A $\beta$ 40 was then added (25–35  $\mu$ L in 10 mM NaOH) to give a final buffer composition identical to that of the isotropic samples and a final volume of 200  $\mu$ L. From a comparison of <sup>1</sup>H–<sup>15</sup>N HSQC spectra, Pf1 caused a slight increase in the pH of the sample at high concentrations. In these cases, the pH was adjusted by the addition of 100 mM HCl, which did not lead to aggregation of A $\beta$ 40 during the experiments. As solutions containing Pf1 had

high viscosity, samples were often left overnight to ensure air bubbles were no longer present. Sample homogeneity in each case was confirmed by the appearance of a sharp doublet in the <sup>2</sup>H one-dimensional spectrum. The quadrupolar splitting in Pf1 solutions was not observed to change particularly over the course of experiments.

**Spin-Labeled Derivatives.** The (1-oxyl-2,2,5,5-tetramethyl- $\Delta$ 3-pyrroline-3-methyl) methanethiosulfonate (MTSL) nitroxide radical was obtained from Toronto Research Chemicals (Toronto, ON) and dissolved by being sonicated in 100 mM sodium phosphate containing 6 M guanidium chloride (pH 8.0) to form a supersaturated solution. Undissolved MTSL was sedimented using a benchtop centrifuge and the supernatant used for subsequent reactions. A $\beta$ 40 cysteine mutants dissolved in 10 mM NaOH (as above) were first reduced *in situ* by an 8-fold excess of tris(2-carboxyethyl)phosphine (TCEP) for 15 min, ensuring the reaction pH remained above 7 by dissolving TCEP in NaOH. The saturated MTSL solution was then added to give a final sodium phosphate concentration of 60 mM, whereupon the reaction with MTSL was allowed to proceed for 15 min.

Matrix-assisted laser desorption ionization mass spectrometry confirmed the presence of the MTSL-labeled species as the major product in the reactions. However, in all mass spectra analyzed, the peak corresponding to unlabeled peptide persisted at a fraction of approximately 10–20% of the total peptide present. An array of different pH values and reaction times were employed, but no significant differences could be detected. Following purification, we checked volumes of <sup>1</sup>H–<sup>15</sup>N HSQC peaks for residues near the labeling site with MTSL in its paramagnetic state. Because of the large PREs at these residues, peak volumes should be undetectably low,<sup>32</sup> which was indeed found to be the case. These results indicate that yields were close to 100% and suggest that peak areas in the mass spectra may be biased by a low mobility of the MTSL-labeled A $\beta$ 40 species.

The reaction mixture was purified by size exclusion chromatography using an analytical Superdex 75 10/300 GL column (GE Healthcare, Amersham, U.K.) eluting with 4 mM sodium phosphate buffer containing 0.1 mM EDTA and 0.004% (w/v) NaN<sub>3</sub> (pH 7.5). Fractions containing A $\beta$ 40 were identified by UV absorbance at 280 nm, and peak areas were used to quantify the amount of peptide present using an extinction coefficient of 1595 cm<sup>–1</sup>. The peptide fractions were lyophilized and redissolved in a 9:1 H<sub>2</sub>O/D<sub>2</sub>O mixture to give a final sodium phosphate concentration of 20 mM. A $\beta$ 40 concentrations in the NMR samples were 60–100  $\mu$ M.

Validation experiments were performed with peptides for which MTSL had been reduced by addition of sodium ascorbate (400  $\mu$ M). The reaction was allowed to proceed for 12 h at 5 °C, and complete reduction was monitored by the increase in intensity of A $\beta$  resonances in the <sup>1</sup>H NMR spectrum. Sodium ascorbate did not lead to any measurable changes in chemical shifts or peak intensities of wild-type A $\beta$ 40 at the concentration used for reduction of the spin-labeled derivatives.

**NMR Spectroscopy.** NMR spectra were recorded on Avance 500 and 700 MHz spectrometers (Bruker BioSpin AG) equipped with four-channel z-gradient cryogenic probes. All experiments were recorded at 278 K. Data were processed using NMRPipe<sup>33</sup> by application of shifted sine bell window functions and extensive zero filling prior to Fourier transformation. Spectra were analyzed with NMRPipe and Sparky

(T. D. Goddard and D. G. Kneller, SPARKY 3, University of California, San Francisco, CA). We found that data acquisition was substantially expedited by the use of a  $^{15}\text{N}$  spectral width of 10.5 ppm. Well-resolved  $^1\text{H}$ – $^{15}\text{N}$  HSQC spectra (Figure S1) could thus be recorded with only 32 complex points in the indirect dimension.

**Residual Dipolar Couplings.**  $^1\text{H}$ – $^{15}\text{N}$  RDCs were derived from the difference in peak splittings between aligned and isotropic samples in two-dimensional IPAP  $^1\text{H}$ – $^{15}\text{N}$  HSQC spectra.<sup>34</sup> Accurate peak positions were determined by fitting a Gaussian function to each peak within Sparky.  $^1D_{\text{NH}}$  values were averaged over three distinct experiments to obtain residue-specific estimates of the standard errors of measurement.

The goodness of fit for each residue in the concentration dependence analysis (see eq 13) was determined by the reduced  $\chi^2$  parameter ( $\chi^2_{\text{red}}$ )

$$\chi^2_{\text{red}} = \frac{1}{\nu} \sum_{i=1}^N \frac{(D_{\text{fit},i} - D_{\text{exp},i})^2}{\sigma_i^2} \quad (1)$$

where  $D_{\text{fit},i}$  and  $D_{\text{exp},i}$  are the fitted and experimental RDC values, respectively,  $\sigma_i$  is the experimental error, and the index  $i$  is the sum runs over the  $N$  concentrations used. The number of degrees of freedom ( $\nu$ ) is given by  $N - n - 1$ , where  $n$  is the number of fitted parameters for each model. A value of  $\chi^2_{\text{red}}$  close to unity indicates that the data are well fitted by the model given the experimental uncertainty.

The agreement between experimental RDCs and those corrected for the effects of alignment-induced perturbation was assessed by the RDC quality factor,<sup>35</sup> which is defined as

$$Q = \sqrt{\frac{\sum_{k=1}^N (D_{\text{corr},k} - D_{\text{exp},k})^2}{\sum_{k=1}^N D_{\text{corr},k}^2}} \quad (2)$$

where  $D_{\text{exp}}$  is the experimental RDC,  $D_{\text{corr}}$  is the corrected RDC corresponding to the unperturbed state, and the index  $k$  runs over all residues for which data were available. Values of  $Q$  below 0.2 are generally thought to indicate good agreement between a predicted quantity (in this case  $D_{\text{exp}}$ ) and its true value (in this case  $D_{\text{corr}}$ ).

**Spin Relaxation.** Backbone  $^{15}\text{N}$  transverse relaxation rates ( $R_2$ ) were measured with a sensitivity-enhanced CPMG pulse sequence that contained additional CPMG trains for heating compensation.<sup>36</sup> Backbone  $^1\text{H}_\text{N}$   $R_2$  rates were measured using the HSQC-based pulse sequence proposed by Kay and co-workers,<sup>32,37</sup> employing a REBURP pulse (3 ms at 500 MHz, centered at 8.3 ppm) for selective refocusing of amide resonances during the first INEPT period. In both cases, 8–10 relaxation delays were recorded in interleaved fashion over the range of 20–700 ms ( $^{15}\text{N}$ ) or 13–223 ms ( $^1\text{H}_\text{N}$ ). Decay curves were fitted with two-parameter single-exponential functions in Sparky, and errors were estimated by the standard deviation of decay constant values upon addition of Gaussian noise to the peak heights (Monte Carlo method).

**Monitoring A $\beta$ 40 Aggregation.**  $^1\text{H}$  NMR experiments were used to assess the aggregation of A $\beta$ 40 peptides over time, as the signal observed in solution NMR comes entirely from the monomeric peptide.<sup>38</sup> To control for any systematic change in spectral intensity over time, which may be caused for example by changes in shims or water suppression, the time evolution of the integral over the A $\beta$ 40 methyl region (0.6–1.0 ppm) was

compared to the integral of the EDTA resonance (3.65 ppm), which is not expected to exhibit time-dependence.

**Diffusion Coefficients.** Translational diffusion coefficients were measured using a stimulated echo pulse sequence<sup>39</sup> that included a 3–9–19 pulse train for effective water suppression.<sup>40</sup> Smooth square gradients were used throughout, with gradient pulse lengths of  $\delta = 4.5$  ms and intergradient delays of  $\Delta = 100$  ms. Spectra were acquired at 32 values of gradient strength ( $G$ ) from 5 to 95% of the maximal value for the probe employed (nominally 53.5 G/cm). The decay of the integral over the aromatic region of the A $\beta$ 40 spectrum (6.9–7.4 ppm) was fitted using a modified form of the Stejskal–Tanner equation suitable for bipolar gradient experiments<sup>39,41</sup>

$$S(G) = S_0 \exp \left[ -G^2 \delta^2 \gamma_{\text{H}}^2 D_t \left( \Delta - \frac{\delta}{3} - \frac{\tau}{2} \right) \right] \quad (3)$$

where  $S_0$  is the signal when  $G = 0$ ,  $\gamma_{\text{H}}$  is the  $^1\text{H}$  gyromagnetic ratio,  $D_t$  is the translational diffusion coefficient, and  $\tau$  is the delay between the two halves of the bipolar gradient (0.17 ms). Average values of  $D_t$  were determined on the basis of three repeats of the experiment on the same sample.

Differences between the diffusion coefficients of the A $\beta$ 40 variants were assessed by statistical testing. In all cases, we employed a significance level of  $\alpha = 0.05$ . Variability was first assessed by a one-way analysis of variance (ANOVA) test. Upon finding significant variability ( $p < \alpha$ ), we performed *post hoc* pairwise comparisons of the paramagnetic variants with the wild-type peptide by unpaired two-tail  $t$  tests. In spite of small sample sizes ( $n = 3$  or 4), the main errors arise from spectral noise and therefore can be assumed to be normally distributed.

The translational diffusion coefficient is related to the hydrodynamic radius ( $R_{\text{H}}$ ) by the Stokes–Einstein relation

$$R_{\text{H}} = \frac{k_{\text{B}} T}{6\pi\eta D_t} \quad (4)$$

where  $k_{\text{B}}$  is the Boltzmann constant,  $T$  is the temperature, and  $\eta$  is the viscosity of the solution. As the temperature and viscosity of solutions containing different A $\beta$ 40 variants are identical, their sizes relative to wild-type A $\beta$ 40 can be calculated as  $R_{\text{H,mut}} = D_{\text{t,wt}}/D_{\text{t,mut}}$ . By using a ratio of diffusion coefficients, it was also not necessary to accurately determine the maximum gradient strength exerted by the probe.

**Chemical Shift Perturbations.** [ $^1\text{H}$ ,  $^{15}\text{N}$ ] weighted chemical shift differences ( $\Delta_{\text{NH}}$ ) between wild-type and spin-labeled peptides were calculated as

$$\Delta_{\text{NH}} = \sqrt{\Delta\delta_{\text{HN}}^2 + \left( \Delta\delta_{\text{N}} \frac{\gamma_{\text{N}}}{\gamma_{\text{H}}} \right)^2} \quad (5)$$

where  $\Delta\delta_{\text{HN}}$  and  $\Delta\delta_{\text{N}}$  are the  $^1\text{H}_\text{N}$  and  $^{15}\text{N}$  chemical shift differences, respectively, and  $\gamma_{\text{H}}$  and  $\gamma_{\text{N}}$  are the  $^1\text{H}_\text{N}$  and  $^{15}\text{N}$  gyromagnetic ratios, respectively. Assignments for the spin-labeled peptides were obtained from HNHA experiments (see the Supporting Information).

**Paramagnetic Relaxation Enhancements.**  $^1\text{H}_\text{N}$  transverse PREs ( $\Gamma_2$ ) were determined from  $^1\text{H}$ – $^{15}\text{N}$  HSQC spectra of A $\beta$ 40 V12C\* in the paramagnetic and diamagnetic states according to the peak volume method proposed by Xue et al.<sup>42</sup>  $\Gamma_2$  was calculated for each residue according to



$$\Gamma_2 = \frac{1}{2\tau} \ln \left( \frac{V_d}{V_p} \right) \quad (6)$$

where  $\tau$  is the length of the INEPT periods ( $1/2J_{\text{NH}}$ ). Volumes were determined by nlinLS Gaussian fitting to the peaks within NMRPipe. A REBURP pulse (1.714 ms at 700 MHz, center at 8.3 ppm) was used in the first INEPT period to refocus only  $^1\text{H}_\text{N}$  spins and avoid intensity modulation by  $^3J_{\text{HNH}\alpha}$ . To ensure equilibration of diamagnetic sample between scans and to avoid underestimation of  $\Gamma_2$  as a result of longitudinal PRE effects, an interscan delay of 4.5 s was used. The effect on peak volumes of sample dilution by addition of sodium ascorbate was taken into account by the addition of a reference compound as suggested by Xue et al.,<sup>42</sup> 100  $\mu\text{M}$  [ $^{15}\text{N}$ ]-N-acetyl-glycine (Isotec, Old Bridge, NJ).

**Calculation of PREs from Protein Structures.** The  $^1\text{H}$  transverse relaxation enhancement in the presence of a paramagnetic species ( $\Gamma_2$ ) is given by the Solomon–Bloembergen equation<sup>43,44</sup>

$$\Gamma_2 = \frac{1}{15} \left( \frac{\mu_0 \gamma_\text{H} g_e \mu_\text{B}}{4\pi} \right)^2 s_e (s_e + 1) [4J(0) + 3J(\omega_\text{H})] \quad (7)$$

where  $J(\omega)$  is the generalized spectral density function for the electron–proton interaction,  $g_e$  is the electron  $g$  factor,  $\gamma_\text{H}$  is the proton gyromagnetic ratio,  $s_e$  is the electron spin quantum number,  $\omega_\text{H}/2\pi$  is the proton Larmor frequency,  $\mu_\text{B}$  is the Bohr magneton, and  $\mu_0$  is the permeability of vacuum. These physical constants are commonly merged into a single constant,  $K$ , which takes a value of  $1.23 \times 10^{16} \text{ Å}^6 \text{ s}^{-2}$  when a nitroxide radical is the paramagnetic group. For proteins containing a paramagnetic group attached by freely rotatable bonds, such as MTSL, the most appropriate form of the spectral density is<sup>45</sup>

$$J(\omega) = \langle r^{-6} \rangle \left[ \frac{S^2 \tau_c}{1 + (\omega \tau_c)^2} + \frac{(1 - S)^2 \tau_t}{1 + (\omega \tau_t)^2} \right] \quad (8)$$

where  $r$  is the electron–proton distance, angle brackets denote averaging over the distribution of distances, and  $S^2$  is the generalized order parameter for the motion of the tagged side chain.  $\tau_c$  is the correlation time for the electron–proton interaction, which can be written as  $(\tau_r^{-1} + \tau_s^{-1})^{-1}$ , where  $\tau_r$  is the rotational correlation time of the molecule and  $\tau_s$  is the electron spin longitudinal relaxation time.  $\tau_t$  is the total correlation time, which can be written as  $(\tau_c^{-1} + \tau_i^{-1})^{-1}$ , where  $\tau_i$  is the correlation time for the internal motion of the spin-label. As  $\tau_s$  is typically 100 times larger than  $\tau_r$  for nitroxide radicals,<sup>46</sup>  $\tau_c$  can be approximated by  $\tau_r$ . Therefore, the spectral density depends on only two correlation times,  $\tau_r$  (overall tumbling) and  $\tau_i$  (internal motions). This treatment assumes that the internal motions of the paramagnetic tag are uncoupled with the rotational tumbling of the macromolecule, with the latter expected to take place on longer time scales.

To evaluate the spectral density (eq 8), it is convenient to decompose  $S^2$  into angular and radial parts

$$S^2 \approx S_\text{ang}^2 S_\text{rad}^2 \quad (9)$$

where the individual parts are given by

$$S_\text{ang}^2 = \frac{4}{5\pi} \sum_{m=2}^2 |Y_m^2(\vartheta, \varphi)|^2 \quad (10)$$

and

$$S_\text{rad}^2 = \frac{\langle r^{-3} \rangle^2}{\langle r^{-6} \rangle} \quad (11)$$

where  $Y_m^2$  values are second-order spherical harmonics and  $(\vartheta, \varphi)$  are the polar and azimuthal angles between the principal axes of the moment of inertia tensor of the molecule and the electron–proton vector for a given conformation of the side chain.

To apply these equations to calculate the PREs from explicit ensembles of A $\beta$ 40, we first generated a library of MTSL rotamers through molecular dynamics simulations of the spin-label attached at position 2 of the peptide. Clustering of the resulting structures led to 76 rotamers for MTSL, which we took to occur with equal likelihood.

For each backbone conformation in the ensemble, the allowed MTSL rotamers were obtained by first aligning the backbone C $\alpha$ , C', and N atoms of residue 12 with those of the MTSL-bearing side chain. All MTSL conformations that produced a steric clash with the A $\beta$ 40 structure were then removed. Clashes were defined to occur when two atoms came within the sum of their van der Waals radii. Xplor-NIH values of the van der Waals radii were used in calculations, with a scaling factor of 0.75 being conventional in the final stages of structure refinement in this package.<sup>47</sup> Only backbone atoms (and C $\beta$ ) were used on A $\beta$ 40 as it is anticipated that side chains could rearrange easily to accommodate MTSL, and in addition, the C $\beta$  atom was excluded from the residue at the labeling site. All atoms on the MTSL side chain were included apart from C $\beta$ , H $\beta$ , and S $\gamma$ . Following the removal of disallowed rotamers,  $\Gamma_2$  was calculated for the backbone conformation using the following correlation time values:  $\tau_r = 3 \text{ ns}$ ,<sup>48</sup> and  $\tau_i = 500 \text{ ps}$ .<sup>22</sup> The PREs were then averaged over all backbone conformations according to

$$\Gamma_2 = \frac{1}{N_s} \sum_{i=1}^{N_s} \Gamma_{2,i} \quad (12)$$

where  $N_s$  is the number of backbone conformations in the ensemble of interest. The separation of averaging over rotamer positions for a specific backbone conformations, and then backbone conformations, assumes that motion of the side chain is faster than and decoupled from backbone conformational changes.

## RESULTS

**RDC Measurements: Possible Perturbations by the Alignment Medium.** The method that we propose for assessing the effects of molecular alignment on RDC measurements of disordered proteins is illustrated in Figure 1. The degree of compatibility of a given protein with a particular alignment medium is first assessed by consideration of the pH, buffer, and temperature requirements.<sup>49</sup> Electrostatic alignment media with charges that are the opposite of that of the protein should be avoided because of the strong attractive forces that will result. More subtle perturbations, however, may arise at a local level around individual residues with charges that are the opposite of that of the alignment medium. Working at high ionic strengths would reduce these perturbations but also increase the correlation between RDCs measured in different alignment media, thus reducing the amount of information that can be extracted from them. Suitable alignment media should, in addition, allow high-resolution spectra to be recorded without extensive line broadening caused by binding<sup>27</sup> or by

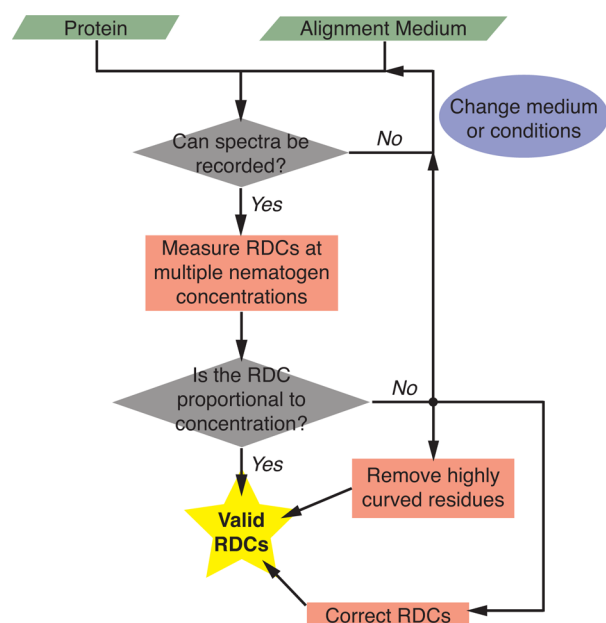


**Figure 1.** Schematic illustration of the method discussed in this work for the measurement of RDCs for disordered proteins. Possible interactions between the protein and the alignment medium (nematogen) are first assessed by measuring NMR spectra. Widespread peak disappearance and sample degradation are indicative of strong interactions. In this case, the solution conditions should be altered or a different medium employed. If NMR spectra of sufficient quality can be recorded,  $^1\text{H}$ – $^{15}\text{N}$  RDCs should be measured over as wide a range of concentrations of the nematogen as practically possible. In the absence of perturbations caused by the alignment medium, the RDC values should be proportional to the concentration. Therefore, RDCs are invalid for residues (denoted as “curved” in the flow diagram) for which significant deviations from linearity are observed. Such residues can be discarded from further analysis or their RDCs corrected according to the procedure described in the text. If RDCs from many residues are subject to perturbations, it may be necessary to change the alignment medium or conditions.

unresolved  $^1\text{H}$ – $^1\text{H}$  dipolar interactions.<sup>50</sup> Strong interactions can be mitigated by using lower concentrations of the alignment media or by screening electrostatic interactions with higher concentrations of salt.<sup>51,52</sup>

Following the optimization of the conditions, the effects of perturbations introduced by the alignment process on the RDCs themselves are elucidated by measuring their values at different nematogen concentrations. In the absence of perturbations, RDC values ( $D$ ) are expected to scale linearly with concentration ( $D = \alpha c$ ), where  $c$  is the concentration and  $\alpha$  is a scaling constant, as the overall anisotropy of the medium increases in proportion to the quantity of nematogen present. Where perturbations occur, provided that the fraction of perturbed molecules is <5%, measured RDC values will show an effective quadratic concentration dependence (see the [Supporting Information](#))

$$D = \alpha c + \beta' c^2 \quad (13)$$

where  $\beta'$  captures the magnitude of the perturbations introduced by the alignment media. Residues showing significant deviations from linear behavior are identified as those showing an increase of >10% in the goodness of fit using the quadratic model versus a linear one. If many residues show high degrees of curvature (i.e., a large value of  $\beta'$ ), this is an

indication that the medium is significantly perturbing the conformational ensemble of the protein and that the medium or the conditions should be altered to record useful RDCs for structural studies. On the other hand, if only a few residues show high curvature, these can be removed and the remaining residues used for subsequent conformational analysis. This approach also allows the corrections needed for the RDCs to be determined, as the RDC value corresponding to the unperturbed state alone is  $\alpha c$ .

**Validity of RDCs for the A $\beta$ 40 Peptide.** We illustrate our method for the validation of RDCs in a study of A $\beta$ 40, a peptide whose aggregation from a disordered monomeric state to form amyloid assemblies is implicated in Alzheimer’s disease.<sup>53</sup> A $\beta$ 40 has a net charge of approximately  $-2.4$  at pH 7.4 ([Figure S2](#)), and therefore, the negatively charged Pf1<sup>50</sup> alignment medium was selected for measurement of RDCs. RDCs from electrostatic alignment can provide valuable information complementary to those commonly recorded in steric media for disordered proteins, and therefore, their use has the potential to expand the amount of RDC data available from these states.<sup>52</sup>

At an ionic strength of 50 mM, use of Pf1 concentrations up to  $\sim 26$  mg/mL yielded NMR spectra of a resolution similar to that of unaligned samples. No NMR signals were broadened beyond detection, and many showed no additional line broadening in the presence of Pf1 ([Figure S3](#)). As these results indicated that conditions were appropriate for RDC measurements, we determined the concentration dependence of the RDC values. Because of the high viscosity of the Pf1 solutions and difficulties in accurate concentration measurement, we used the  $^2\text{H}$  quadrupolar splitting ( $Q_{\text{cc}}$ ) as an *in situ* measure of Pf1 concentration. The two are directly proportional when Pf1 is fully aligned,<sup>51</sup> a situation that was confirmed in this study by the identical values of  $Q_{\text{cc}}$  for the lowest Pf1 concentration at two magnetic field strengths (11.7 and 16.4 T).

Goodness-of-fit tests for the quadratic and linear concentration dependence models are shown in [Figure 2a](#), where a lower  $\chi^2_{\text{red}}$  value indicates an improved fit to the data for the quadratic model; because the statistics are normalized for the number of model parameters, the reductions in  $\chi^2_{\text{red}}$  are not simply a result of increased model complexity. A number of residues show improved agreement with the quadratic model, and the three examples of residues exhibiting pronounced curvature are shown in [Figure 2b](#). The dashed lines in the plots show the RDC values of the unperturbed state, indicating that alignment-induced perturbations lead to measurable systematic deviations in RDC values.

The largest curvatures are observed at residues K16 and N27, which suggest that perturbations may arise from transient binding of A $\beta$ 40 to the negatively charged Pf1 surface ([Figure 2c](#)) as N27 is adjacent to the other lysine residue in the A $\beta$ 40 sequence (K28). To determine whether binding was significant in this case, backbone  $^{15}\text{N}$  transverse relaxation rates ( $R_2$ ) were measured in the presence and absence of Pf1.  $R_2$  values are expected to increase for residues involved in binding to Pf1 because of the very fast transverse relaxation of spins tumbling with the viral particle that has an estimated correlation time on the order of 1–100  $\mu\text{s}$ .<sup>54</sup>

[Figure 2d](#) shows the changes in  $R_2$  upon addition of  $\sim 26$  mg/mL Pf1 to the solution containing the A $\beta$ 40 peptide. The largest increases occur between residues K16 and F20, indicating that binding to Pf1 occurs principally through this region. In contrast, increases in  $R_2$  are not observed in the

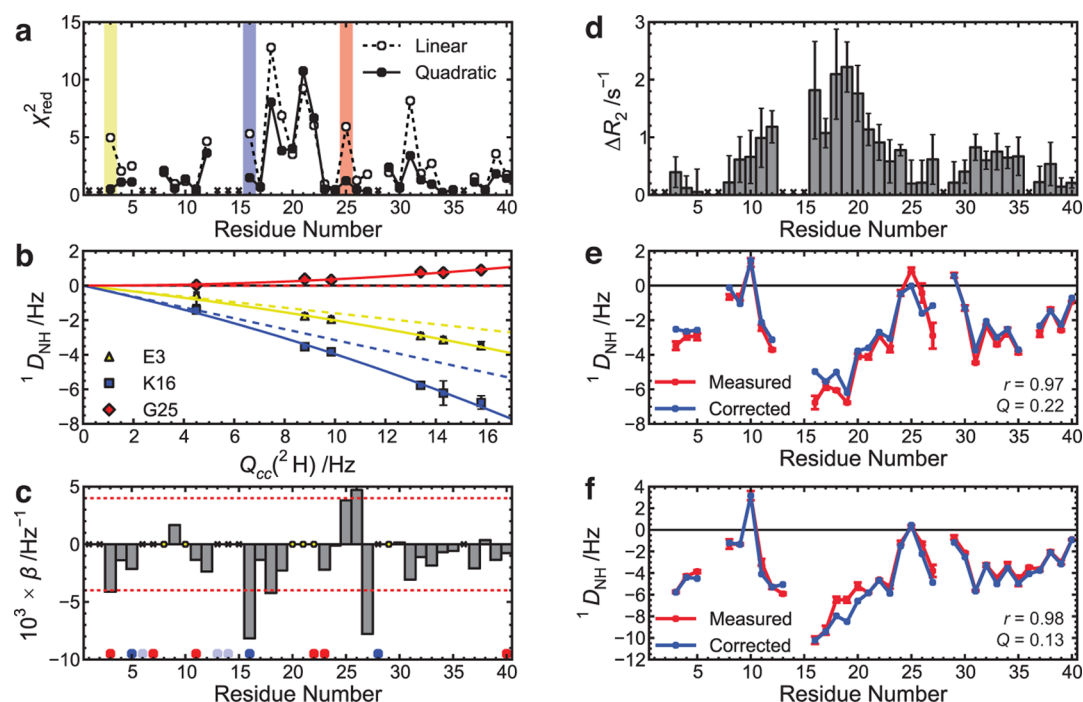


**Figure 2.** Concentration dependence of RDCs measured for the Aβ40 peptide. This analysis reveals a slight perturbation of the Aβ40 conformational ensemble induced by Pf1 under the conditions used in this study. (a) Reduced  $\chi^2$  values for fits of the RDC data to linear and quadratic models (see the text), showing improvements upon addition of the quadratic term that are not merely the result of increased model complexity; colored bars refer to the three residues in panel b. (b)  $^1H$ – $^{15}N$  RDC values for three residues as a function of the  $^2H$  quadrupolar splitting,  $Q_{cc}(^2H)$ , which is proportional to the concentration of Pf1.<sup>51,62</sup> Solid lines are quadratic fits to the data; dashed lines are the linear term from the fit, corresponding to the RDC values of the unperturbed state. (c) Errors in the RDC values given by the coefficient of the quadratic term in eq 13. Because we used quadrupolar splittings instead of concentrations, the curvature is indicated by  $\beta$ , rather than by  $\beta'$  as in eq 13. Negatively and positively charged amino acids are denoted by red and blue circles, respectively, and histidine residues are shown by pale blue circles that indicate their degree of protonation at the given pH. Red dashed lines indicate the value of  $\beta$  above which residues are excluded from analysis because they would be affected by an error of >1 Hz at a quadrupolar splitting of 15.8 Hz. Six residues did not show significant improvement in  $\chi^2_{red}$  upon addition of a quadratic term (yellow circles). (d) Changes in  $^{15}N$  transverse relaxation rates ( $\Delta R_2$ ) upon addition of Pf1. Residues for which no data are available are marked with crosses (×). (e) Comparison of measured RDCs at  $Q_{cc} = 15.8$  Hz and corrected RDCs obtained from the linear terms of the quadratic fits shown in panel b. (f) Comparison of measured and corrected RDCs from a second set of concentration dependence experiments performed in the presence of an additional 150 mM NaCl at  $Q_{cc} = 18.4$  Hz.

proximity of K28, indicating that this region does not bind to Pf1 directly. The perturbation of the RDC values between residues G25 and N27 may therefore arise due to stabilization of turn conformations upon binding to Pf1, but with the residues at the head of the turn not directly in contact with the surface of the bacteriophage. Turn formation has previously been shown to cause a change in sign in the RDC profiles,<sup>55</sup> which is present here in the measured RDCs at residue G25, but not in the corrected RDCs corresponding to the unperturbed conformations alone, indicating that turn formation is less common within the native ensemble (Figure 2e).

The effects of the systematic errors introduced by Pf1 on the RDC profile of Aβ40 can be seen by a comparison of corrected and measured data at  $Q_{cc} = 15.8$  Hz (Figure 2e). Overall, the correlation between the two sets of RDCs is high ( $r = 0.97$ ), and the RDC Q factor (see Materials and Methods) has a value of 0.22. Nevertheless, significant deviations can be observed in several regions, and five residues show errors of >1 Hz. Removal of these residues reduces the Q factor to 0.13.

We also repeated the concentration dependence analysis for RDCs at an ionic strength of 200 mM and found that systematic errors were reduced ( $Q = 0.13$  with all residues included), particularly at residues K16 and N27 (Figure 2f and Figure S4). These findings provide further support for the hypothesis that binding between the Aβ40 peptide and Pf1 is

mediated by electrostatic interactions and show that RDC concentration dependence measurements are able to identify whether conformational changes are taking place with high sensitivity.

**PRE Measurements: Possible Perturbations from Paramagnetic Tagging.** We next investigated a method for validation of paramagnetic derivatives to be used in PRE measurements. The method, which is outlined in Figure 3, involves detailed comparison of the tagged variant with the properties of the unmodified protein, with a particular emphasis on determining the effect of paramagnetic tagging on long-range structure within the conformational ensemble. Candidate sites for tagging can be selected on the basis of their positions in the sequence (e.g., solvent exposure and location outside highly structured regions) and to match the physicochemical properties of the final paramagnetic group. Because many nitroxide-based spin-labels are hydrophobic, they should be substituted for large, nonpolar side chains. On the other hand, metal-chelating moieties often contain amide or carboxylic acid functional groups; therefore, similar polar side chains should be selected for tagging.<sup>23</sup>

Following successful production and tagging, each variant is compared to the unmodified protein using three criteria, which are considered in sequence by starting from the least sample intensive and time-consuming ones. The first step is to establish



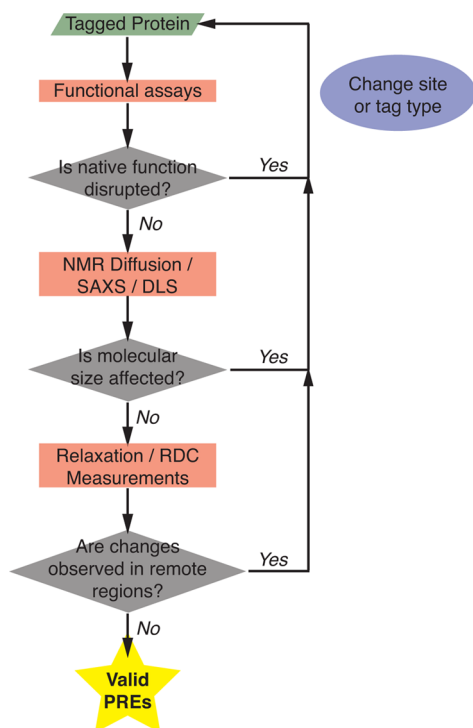


**Figure 3.** Schematic illustration of the method discussed in this work for the measurement of PREs for disordered proteins. Following the production and paramagnetic tagging of the protein, the first stage is to perform functional assays to ensure the presence of the tag does not abrogate native function. If this is not the case, it is then particularly important to ascertain the effect of spin labeling on the molecular dimensions via the measurement of the radius of gyration ( $R_g$ ) or the hydrodynamic radius ( $R_H$ ). Variants that successfully pass through this stage should be produced with appropriate isotopic enrichment and tested for deviations in  $^{15}\text{N}$  transverse relaxation rates ( $R_2$ ) or, more conclusively,  $^1\text{H}$ – $^{15}\text{N}$  RDCs. These measurements give an indication of whether the spin-label affects long-range contacts within the protein, which would preclude the use of that variant in PRE measurements.

that native functions are preserved upon derivatization, as a loss of these is indicative of changes in important structural features. Being sensitive to long-range distances (10–35 Å), PREs are expected to be strongly affected by changes in the compactness of the polypeptide chain. Therefore, the second step in the method is to assess the effect of tagging on the global dimensions of the protein, through either NMR diffusion or dynamic light scattering (DLS) measurements, which allow comparison of hydrodynamic radii ( $R_H$ ), or small-angle X-ray scattering (SAXS), for comparison of radii of gyration ( $R_g$ ). In the final stage, heteronuclear NMR experiments are used to probe the effect of paramagnetic tagging at the residue-specific level. Very useful parameters for the comparison are  $^{15}\text{N}$   $R_2$  rates and, where possible,  $^1\text{H}$ – $^{15}\text{N}$  RDCs, both of which are sensitive to long-range structure within disordered proteins.<sup>22,56</sup> Changes in these parameters should decrease further from the tagging site, with no changes observed in remote regions.

**Validation of Paramagnetic A $\beta$ 40 Variants for PRE Measurements.** The use of the method is again illustrated in the study of the A $\beta$ 40 peptide, where we selected three positions for mutation of the native amino acid to cysteine and subsequent paramagnetic tagging by the thiol-specific nitroxide radical MTSL<sup>57</sup> (Figure 4a). Mutations were made outside the A $\beta$ 40 fibril core regions (gray arrows, Figure 4a), avoiding

charged and aromatic residues. As a functional test, we monitored the aggregation rates of the tagged peptides (A $\beta$ \*) by  $^1\text{H}$  NMR. Because during solution NMR, the A $\beta$  signals have been shown to arise entirely from the monomeric peptide,<sup>38</sup> a loss of signal corresponds to the conversion of monomeric A $\beta$ 40 into higher-molecular weight species. Over the period studied, wild-type A $\beta$ 40 does not aggregate, a trend that is followed by the V12C\* and S26C\* variants (Figure 4b). However, the magnitude of the A2C\* signal drops by 13%, indicating some aggregation for this peptide. An increase in the level of aggregation, by itself, does not necessarily imply an alteration of the monomeric conformational ensemble,<sup>58</sup> as it may result from a variety of other microscopic processes contributing to the overall aggregation process.<sup>6,59</sup> However, aggregation over this period does preclude accurate measurement of PREs, as intensity changes between paramagnetic and diamagnetic samples are no longer solely caused by the proximity to the paramagnetic group. As a result, the use of the A2C\* mutant was not considered for further analysis.

To assess the effects of MTSL labeling on the overall dimensions of the A $\beta$ 40 peptide, diffusion coefficients were measured by NMR and used to determine the relative hydrodynamic radii ( $R_H$ ) for each peptide relative to that of the wild type (Figure 4c). The results exhibited significant variability, as also indicated by a one-way ANOVA test, which gave a  $p$  value of 0.011. Post hoc unpaired  $t$  tests (two-tail;  $\alpha = 0.05$ ;  $n \geq 3$ ) indicated identical values for the wild type and V12C\* ( $p = 0.57$ ), whereas the wild type and S26C\* were significantly different ( $p = 0.024$ ). As alteration of the compactness of the S26C\* peptide may affect PRE measurements, it was excluded from further analysis.

A final assessment of the suitability of the V12C\* variant was performed using heteronuclear NMR experiments. The local effects caused by the introduction of a reduced MTSL spin-label at position 12 were monitored using  $^{15}\text{N}$   $R_2$  rates, which show the largest differences between the wild type and V12C\* variants in the region of S8–F20 (Figure 4d), with higher values for V12C\* indicative of a decrease in segmental diffusion rate as a result of the introduction of the bulky spin-label. These results were also confirmed by  $^1\text{H}$ – $^{15}\text{N}$  RDCs measured in Pfl medium (Figure 4e), which show changes over a similar region (E11–E22) and none in remote regions. The V12C\* derivative therefore satisfies our criteria as a valid model of wild-type A $\beta$ 40 for use in PRE measurements.

We also measured [ $^1\text{H}$ ,  $^{15}\text{N}$ ] weighted chemical shift differences ( $\Delta_{\text{NH}}$ ) between wild-type and spin-labeled peptides, which are typically used to assess the effects of paramagnetic tagging (Figure 4f). Changes are much smaller than those measured by relaxation rates and RDCs, though there are some small changes in the region of F19–A21 detected for the V12C\* variant.  $\Delta_{\text{NH}}$  values for the S26C\* variant are local and similar in magnitude to that of V12C\* despite the expansion of the ensemble observed for this peptide, which underlines the importance of the  $R_H$  measurements. For both peptides,  $^1\text{H}\alpha$  chemical shifts and  $^3J_{\text{HNH}\alpha}$  measurements showed even smaller changes with respect to that of wild-type A $\beta$ 40 (Figure S5); these parameters are therefore also of limited use for assessing the effect of paramagnetic tagging on the conformations of disordered proteins.

## DISCUSSION AND CONCLUSIONS

RDCs and PREs have recently emerged as powerful NMR observables for the high-resolution characterization of disor-

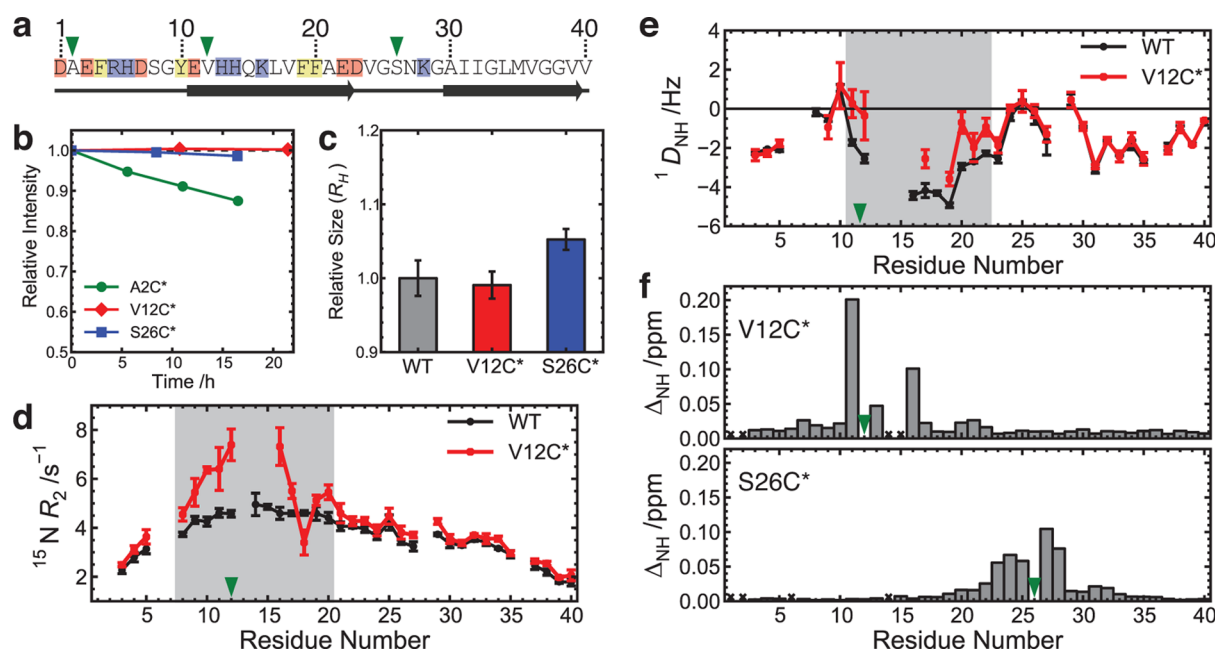


**Figure 4.** Validation of the paramagnetic derivatives of the A $\beta$ 40 peptide for PRE experiments. (a) Sequence of wild-type A $\beta$ 40 showing sites chosen for cysteine mutation and spin labeling (green triangles). Charged (red and blue) and aromatic (yellow) residues were excluded, as were those in core region of A $\beta$ 40 amyloid fibrils<sup>63</sup> (gray arrows). (b) Stability of spin-labeled A $\beta$  variants monitored by the integral over the methyl region of the  $^1\text{H}$  NMR spectrum. A2C\* variant aggregates during the 16 h period required to perform PRE experiments. (c) Relative hydrodynamic radii of the different A $\beta$  variants determined from NMR diffusion measurements, showing a significant increase in the case of the S26C\* variant. (d)  $^{15}\text{N}$  transverse relaxation rates compared between wild-type A $\beta$ 40 and the V12C\* variant. Major differences are observed around the site of labeling (green triangle). (e)  $^1\text{H}$ - $^{15}\text{N}$  RDCs for wild-type A $\beta$ 40 and the V12C\* variant also exclusively show differences in the proximity of the spin labeling site (gray shaded region). (f) Both relaxation rates and RDCs are much more sensitive to spin labeling than  $[\text{H}, \text{N}]$  weighted chemical shift perturbations ( $\Delta_{\text{NH}}$ ), which are typically used to assess the effects of spin labeling.  $\Delta_{\text{NH}}$  values ( $<0.03$ ) are also comparable to noise and highly localized for the S26C\* variant, highlighting the importance of measurement of the global dimensions of the protein for validation.

dered proteins.<sup>9–11,13,14,17,18,20–23</sup> These two types of data can be back-calculated readily from ensembles of structures and are particularly useful as they both contain long-range distance information, in contrast to other parameters such as chemical shifts, NOEs, and scalar couplings. The combination of RDCs and PREs as structural restraints is also particularly advantageous as it makes use of their different dependence on the conformations of the protein.<sup>14</sup> This aspect is illustrated in Figure 5, where a schematic distribution of the radius of gyration in the conformational ensemble of a typical disordered protein is shown, along with bars indicating the contribution that each part of the distribution makes to measured RDC and PRE data. PREs, because they are highly sensitive to short distances because of their  $\langle r^{-6} \rangle$  dependence, can provide important information about the nature of compact states within the ensemble. On the other hand, RDCs show a much weaker dependence on the radius of gyration, but the alignment magnitude is largest for conformers with a high aspect ratio,<sup>60</sup> making them more sensitive than PREs to extended conformations.

To measure RDCs or PREs, a protein must be either exposed to a non-native environment, namely the alignment medium, or subjected to non-native covalent modification, such as attachment of a nitroxide spin-label. In an effort to assess the effects of these changes, we have described experimental methods that can be applied to validate the measurement of RDCs and PREs. We anticipate that they will be particularly useful for the study of disordered proteins and other highly dynamic protein states, as they do not rely on prior structural knowledge. Furthermore, they can be applied independently for each medium or tagging

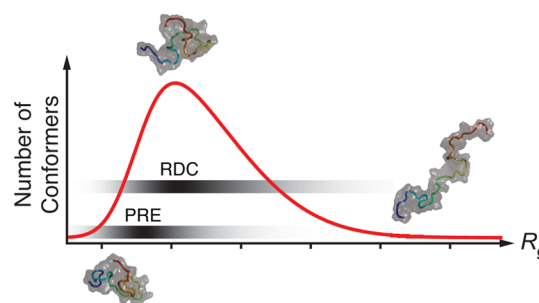


**Figure 5.** Schematic illustration of a typical distribution of the radius of gyration ( $R_g$ ) for a disordered protein. Representative conformers of a typical disordered protein are shown as ribbon diagrams. Gray shaded bars indicate the weights of the contributions that conformers with a particular  $R_g$  value make to the observed NMR signal. These weights depend on the magnitude of the RDCs or PREs expected for a conformer with that value of  $R_g$  and the number of conformers with that size in the ensemble. PREs are particularly sensitive to compact species,<sup>14</sup> whereas RDCs have a weaker size dependence but are largest for conformations with a high aspect ratio.<sup>60</sup> As a result, the two techniques provide a complementary coverage of the conformational space of a protein.

site and do not rely on potentially ambiguous cross-validation of multiple data sets, which is a limitation of current structure-free RDC validation protocols.<sup>61</sup>

The RDC validation method that we have discussed allows data to be corrected for the effects of the alignment medium, yielding the RDCs corresponding in principle to the unperturbed state. If RDCs from multiple bond vectors are



required and several concentration dependence series are too time-consuming, data from residues identified as invalid from the analysis of  $^1\text{H}$ – $^{15}\text{N}$  RDCs can be removed from all sets, yielding valid couplings from multiple bond vectors. This method can be applied to RDCs recorded in any alignment medium provided that (i) the protein can be aligned over a sufficient range of concentrations such that RDC variations can be detected above measurement errors, (ii) line broadening is not too severe at high concentrations that it precludes accurate RDC measurements, and (iii) the order parameter of the nematogen remains constant over this concentration range. The latter can be verified by linear variation of the  $^2\text{H}$  quadrupolar splitting of the  $\text{D}_2\text{O}$  resonance over the concentration range studied. On the basis of a survey of currently available media, these criteria are satisfied by most systems used for weak alignment of proteins. Provided the alignment medium is amenable to dilution, the concentration dependence series can be obtained by preparation of a single protein sample at a high nematogen concentration, followed by successive dilution. However, for samples in anisotropic gels, it is necessary to prepare a separate protein sample at each gel concentration. Strained polyacrylamide gels, which are commonly used for recording RDCs of disordered proteins, may also provide additional complications as the alignment of the samples depends on both the concentration of acrylamide and the degree of compression applied to the gel. The former may be subject to uncertainties if the gel is only partially rehydrated after drying, and the latter has been found to vary substantially in our hands as evidenced by  $\sim 30\%$  variability in the  $^2\text{H}$  quadrupolar splitting for samples containing identical acrylamide concentrations.

The PRE validation method represents a stringent quality control of possible sites for paramagnetic tagging, which should lead to increased confidence in the reliability of PRE data from disordered proteins. Application of the method to A $\beta$ 40 shows that substantial changes can result from spin labeling and highlights the importance of validation using measurements that report on changes in long-range structure. It should be noted, however, that as none of the techniques used have a sensitivity comparable to that of PREs for detecting the presence of low population states,<sup>23</sup> the method that we have presented cannot rule out small population shifts caused by the paramagnetic groups. These changes may nevertheless manifest themselves in the PREs, especially if the conformations favored are more compact than in the unmodified protein. It is not clear at present how this limitation can be overcome experimentally, and it is therefore inevitable that PRE measurements must be subjected to consistency checks with other experimental data or with PREs from different labeling sites.

In conclusion, we anticipate that the quantitative assessment of the systematic errors associated with RDC and PRE measurements using the strategies discussed in this work will expand the range of applicability of these NMR parameters for the structural characterization at high resolution of disordered states of proteins that are increasingly being recognized as being of considerable biological interest and significance.

## ■ ASSOCIATED CONTENT

### ■ Supporting Information

The Supporting Information is available free of charge on the ACS Publications website at DOI: 10.1021/acs.biochem.5b00670.

Methods, supporting results and discussion, and four supporting figures (PDF)

## ■ AUTHOR INFORMATION

### Corresponding Author

\*Department of Chemistry, University of Cambridge, Cambridge CB2 1EW, U.K. E-mail: mv245@cam.ac.uk. Phone: +44 1223 763873.

### Funding

This work was partly supported by the Wellcome Trust and BBSRC (CMD and MV), the JSPS/MEXT Grants in Aid for Scientific Research on Innovation Areas (25102008 to M.Y.-U.), and Grants-in-Aid for Scientific Research (A) (15H02491 to M.Y.U.) and Young Scientists (B) (15K21680 to M.Y.U.). M.Y.U. is a recipient of the Naito Foundation Grant for Studying Overseas.

### Notes

The authors declare no competing financial interest.

## ■ REFERENCES

- (1) Wright, P. E., and Dyson, H. J. (2014) Intrinsically disordered proteins in cellular signalling and regulation. *Nat. Rev. Mol. Cell Biol.* 16, 18–29.
- (2) van der Lee, R., Buljan, M., Lang, B., Weatheritt, R. J., Daughdrill, G. W., Dunker, A. K., Fuxreiter, M., Gough, J., Gsponer, J., Jones, D. T., et al. (2014) Classification of intrinsically disordered regions and proteins. *Chem. Rev.* 114, 6589–6631.
- (3) Uversky, V. N. (2013) A decade and a half of protein intrinsic disorder: biology still waits for physics. *Protein Sci.* 22, 693–724.
- (4) Tompa, P. (2012) Intrinsically disordered proteins: a 10-year recap. *Trends Biochem. Sci.* 37, 509–516.
- (5) Habchi, J., Tompa, P., Longhi, S., and Uversky, V. N. (2014) Introducing protein intrinsic disorder. *Chem. Rev.* 114, 6561–6588.
- (6) Knowles, T. P., Vendruscolo, M., and Dobson, C. M. (2014) The amyloid state and its association with protein misfolding diseases. *Nat. Rev. Mol. Cell Biol.* 15, 384–396.
- (7) Heller, G. T., Sormanni, P., and Vendruscolo, M. (2015) Targeting disordered proteins with small molecules using entropy. *Trends Biochem. Sci.* 40, 491–496.
- (8) Varadi, M., Kosol, S., Lebrun, P., Valentini, E., Blackledge, M., Dunker, A. K., Felli, I. C., Forman-Kay, J. D., Kriwacki, R. W., Pierattelli, R., et al. (2014) pE-DB: a database of structural ensembles of intrinsically disordered and of unfolded proteins. *Nucleic Acids Res.* 42, D326–D335.
- (9) Lindorff-Larsen, K., Kristjansdottir, S., Teilum, K., Fieber, W., Dobson, C. M., Poulsen, F. M., and Vendruscolo, M. (2004) Determination of an ensemble of structures representing the denatured state of the bovine acyl-coenzyme A binding protein. *J. Am. Chem. Soc.* 126, 3291–3299.
- (10) Dedmon, M. M., Lindorff-Larsen, K., Christodoulou, J., Vendruscolo, M., and Dobson, C. M. (2005) Mapping long-range interactions in  $\alpha$ -synuclein using spin-label NMR and ensemble molecular dynamics simulations. *J. Am. Chem. Soc.* 127, 476–477.
- (11) Bertoni, C. W., Jung, Y.-S., Fernandez, C. O., Hoyer, W., Griesinger, C., Jovin, T. M., and Zweckstetter, M. (2005) Release of long-range tertiary interactions potentiates aggregation of natively unstructured  $\alpha$ -synuclein. *Proc. Natl. Acad. Sci. U. S. A.* 102, 1430–1435.
- (12) Mittag, T., and Forman-Kay, J. D. (2007) Atomic-level characterization of disordered protein ensembles. *Curr. Opin. Struct. Biol.* 17, 3–14.
- (13) Nodet, G., Salmon, L. C., Ozenne, V., Meier, S., Jensen, M. R., and Blackledge, M. (2009) Quantitative description of backbone conformational sampling of unfolded proteins at amino acid resolution from NMR residual dipolar couplings. *J. Am. Chem. Soc.* 131, 17908–17918.

- (14) Huang, J.-R., and Grzesiek, S. (2010) Ensemble calculations of unstructured proteins constrained by RDC and PRE data: a case study of urea-denatured ubiquitin. *J. Am. Chem. Soc.* 132, 694–705.
- (15) Smith, L. J., Bolin, K. A., Schwalbe, H., MacArthur, M. W., Thornton, J. M., and Dobson, C. M. (1996) Analysis of main chain torsion angles in proteins: prediction of NMR coupling constants for native and random coil conformations. *J. Mol. Biol.* 255, 494–506.
- (16) Camilloni, C., and Vendruscolo, M. (2014) Statistical mechanics of the denatured state of a protein using replica-averaged metadynamics. *J. Am. Chem. Soc.* 136, 8982–8991.
- (17) Jensen, M. R., Markwick, P. R., Meier, S., Griesinger, C., Zweckstetter, M., Grzesiek, S., Bernadó, P., and Blackledge, M. (2009) Quantitative determination of the conformational properties of partially folded and intrinsically disordered proteins using NMR dipolar couplings. *Structure* 17, 1169–1185.
- (18) Esteban-Martín, S., Fenwick, R. B., and Salvatella, X. (2010) Refinement of ensembles describing unstructured proteins using NMR residual dipolar couplings. *J. Am. Chem. Soc.* 132, 4626–4632.
- (19) Camilloni, C., and Vendruscolo, M. (2015) A tensor-free method for the structural and dynamical refinement of proteins using residual dipolar couplings. *J. Phys. Chem. B* 119, 653–661.
- (20) Allison, J. R., Varnai, P., Dobson, C. M., and Vendruscolo, M. (2009) Determination of the free energy landscape of  $\alpha$ -synuclein using spin label nuclear magnetic resonance measurements. *J. Am. Chem. Soc.* 131, 18314–18326.
- (21) Felitsky, D. J., Lietzow, M. A., Dyson, H. J., and Wright, P. E. (2008) Modeling transient collapsed states of an unfolded protein to provide insights into early folding events. *Proc. Natl. Acad. Sci. U. S. A.* 105, 6278–6283.
- (22) Salmon, L. C., Nodet, G., Ozenne, V., Yin, G., Jensen, M. R., Zweckstetter, M., and Blackledge, M. (2010) NMR characterization of long-range order in intrinsically disordered proteins. *J. Am. Chem. Soc.* 132, 8407–8418.
- (23) Clore, G. M., and Iwahara, J. (2009) Theory, practice, and applications of paramagnetic relaxation enhancement for the characterization of transient low-population states of biological macromolecules and their complexes. *Chem. Rev.* 109, 4108–4139.
- (24) Fawzi, N. L., Ying, J., Torchia, D. A., and Clore, G. M. (2010) Kinetics of amyloid  $\beta$  monomer-to-oligomer exchange by NMR relaxation. *J. Am. Chem. Soc.* 132, 9948–9951.
- (25) Tjandra, N., and Bax, A. (1997) Direct measurement of distances and angles in biomolecules by NMR in a dilute liquid crystalline medium. *Science* 278, 1111–1114.
- (26) Tolman, J., Flanagan, J., Kennedy, M. A., and Prestegard, J. (1995) Nuclear magnetic dipole interactions in field-oriented proteins: information for structure determination in solution. *Proc. Natl. Acad. Sci. U. S. A.* 92, 9279–9283.
- (27) Dahlke Ojennus, D. D., Mitton-Fry, R. M., and Wuttke, D. S. (1999) Induced alignment and measurement of dipolar couplings of an SH2 domain through direct binding with filamentous phage. *J. Biomol. NMR* 14, 175–179.
- (28) Goto, N. K., Skrynnikov, N. R., Dahlquist, F. W., and Kay, L. E. (2001) What is the average conformation of bacteriophage T4 lysozyme in solution? A domain orientation study using dipolar couplings measured by solution NMR. *J. Mol. Biol.* 308, 745–764.
- (29) Lukin, J. A., Kontaxis, G., Simplaceanu, V., Yuan, Y., Bax, A., and Ho, C. (2003) Quaternary structure of hemoglobin in solution. *Proc. Natl. Acad. Sci. U. S. A.* 100, 517–520.
- (30) Meier, S., Blackledge, M., and Grzesiek, S. (2008) Conformational distributions of unfolded polypeptides from novel NMR techniques. *J. Chem. Phys.* 128, 052204.
- (31) Vendruscolo, M. (2007) Determination of conformationally heterogeneous states of proteins. *Curr. Opin. Struct. Biol.* 17, 15–20.
- (32) Iwahara, J., Tang, C., and Marius Clore, G. (2007) Practical aspects of  $^1\text{H}$  transverse paramagnetic relaxation enhancement measurements on macromolecules. *J. Magn. Reson.* 184, 185–195.
- (33) Delaglio, F., Grzesiek, S., Vuister, G. W., Zhu, G., Pfeifer, J., and Bax, A. (1995) NMRPipe: a multidimensional spectral processing system based on UNIX pipes. *J. Biomol. NMR* 6, 277–293.
- (34) Ottiger, M., Delaglio, F., and Bax, A. (1998) Measurement of Dipolar Couplings from Simplified Two-Dimensional NMR Spectra. *J. Magn. Reson.* 131, 373–378.
- (35) Cornilescu, G., Marquardt, J. L., Ottiger, M., and Bax, A. (1998) Validation of protein structure from anisotropic carbonyl chemical shifts in a dilute liquid crystalline phase. *J. Am. Chem. Soc.* 120, 6836–6837.
- (36) Farrow, N. A., Muhandiram, R., Singer, A. U., Pascal, S. M., Kay, C. M., Gish, G., Shoelson, S. E., Pawson, T., Forman-Kay, J. D., and Kay, L. E. (1994) Backbone dynamics of a free and a phosphopeptide-complexed Src homology 2 domain studied by  $^{15}\text{N}$  NMR relaxation. *Biochemistry* 33, 5984–6003.
- (37) Donaldson, L. W., Skrynnikov, N. R., Choy, W.-Y., Muhandiram, D. R., Sarkar, B., Forman-Kay, J. D., and Kay, L. E. (2001) Structural characterization of proteins with an attached ATCUN motif by paramagnetic relaxation enhancement NMR spectroscopy. *J. Am. Chem. Soc.* 123, 9843–9847.
- (38) Hou, L., Shao, H., Zhang, Y., Li, H., Menon, N. K., Neuhaus, E. B., Brewer, J. M., Byeon, I.-J. L., Ray, D. G., Vitek, M. P., et al. (2004) Solution NMR studies of the  $\text{A}\beta$  (1–40) and  $\text{A}\beta$  (1–42) peptides establish that the Met35 oxidation state affects the mechanism of amyloid formation. *J. Am. Chem. Soc.* 126, 1992–2005.
- (39) Wu, D., Chen, A., and Johnson, C. (1995) Flow imaging by means of  $^{1\text{D}}$  pulsed-field-gradient NMR with application to electroosmotic flow. *J. Magn. Reson., Ser. A* 115, 123–126.
- (40) Sklenar, V., Piatto, M., Leppik, R., and Saudek, V. (1993) Gradient-tailored water suppression for  $^1\text{H}$ - $^{15}\text{N}$  HSQC experiments optimized to retain full sensitivity. *J. Magn. Reson., Ser. A* 102, 241–245.
- (41) Stejskal, E., and Tanner, J. (1965) Spin diffusion measurements: spin echoes in the presence of a time-dependent field gradient. *J. Chem. Phys.* 42, 288–292.
- (42) Xue, Y., Podkorytov, I. S., Rao, D. K., Benjamin, N., Sun, H., and Skrynnikov, N. R. (2009) Paramagnetic relaxation enhancements in unfolded proteins: Theory and application to drkN SH3 domain. *Protein Sci.* 18, 1401–1424.
- (43) Solomon, I. (1955) Relaxation processes in a system of two spins. *Phys. Rev.* 99, 559.
- (44) Bloembergen, N., and Morgan, L. (1961) Proton relaxation times in paramagnetic solutions. Effects of electron spin relaxation. *J. Chem. Phys.* 34, 842–850.
- (45) Iwahara, J., Schwieters, C. D., and Clore, G. M. (2004) Ensemble approach for NMR structure refinement against  $^1\text{H}$  paramagnetic relaxation enhancement data arising from a flexible paramagnetic group attached to a macromolecule. *J. Am. Chem. Soc.* 126, 5879–5896.
- (46) Gillespie, J. R., and Shortle, D. (1997) Characterization of long-range structure in the denatured state of staphylococcal nuclease. I. Paramagnetic relaxation enhancement by nitroxide spin labels. *J. Mol. Biol.* 268, 158–169.
- (47) Schwieters, C. D., Kuszewski, J. J., and Mariusclore, G. M. (2006) Using Xplor-NIH for NMR molecular structure determination. *Prog. Nucl. Magn. Reson. Spectrosc.* 48, 47–62.
- (48) Danielsson, J., Andersson, A., Jarvet, J., and Gräslund, A. (2006)  $^{15}\text{N}$  relaxation study of the amyloid  $\beta$ -peptide: structural propensities and persistence length. *Magn. Reson. Chem.* 44, S114–S121.
- (49) Chen, K., and Tjandra, N. (2011) The use of residual dipolar coupling in studying proteins by NMR. *Top. Curr. Chem.* 326, 47–67.
- (50) Hansen, M. R., Mueller, L., and Pardi, A. (1998) Tunable alignment of macromolecules by filamentous phage yields dipolar coupling interactions. *Nat. Struct. Biol.* 5, 1065–1074.
- (51) Zweckstetter, M., and Bax, A. (2001) Characterization of molecular alignment in aqueous suspensions of Pf1 bacteriophage. *J. Biomol. NMR* 20, 365–377.
- (52) Skora, L., Cho, M. K., Kim, H. Y., Becker, S., Fernandez, C. O., Blackledge, M., and Zweckstetter, M. (2006) Charge-Induced Molecular Alignment of Intrinsically Disordered Proteins. *Angew. Chem., Int. Ed.* 45, 7012–7015.

- (53) Haass, C., and Selkoe, D. J. (2007) Soluble protein oligomers in neurodegeneration: lessons from the Alzheimer's amyloid  $\beta$ -peptide. *Nat. Rev. Mol. Cell Biol.* 8, 101–112.
- (54) Tsang, P., and Opella, S. (1986) Pfl virus particle dynamics. *Biopolymers* 25, 1859–1864.
- (55) Mukrasch, M. D., Markwick, P., Biernat, J., von Bergen, M., Bernadó, P., Griesinger, C., Mandelkow, E., Zweckstetter, M., and Blackledge, M. (2007) Highly populated turn conformations in natively unfolded tau protein identified from residual dipolar couplings and molecular simulation. *J. Am. Chem. Soc.* 129, 5235–5243.
- (56) Klein-Seetharaman, J., Oikawa, M., Grimshaw, S. B., Wirmer, J., Duchardt, E., Ueda, T., Imoto, T., Smith, L. J., Dobson, C. M., and Schwalbe, H. (2002) Long-range interactions within a nonnative protein. *Science* 295, 1719–1722.
- (57) Berliner, L. J., Grunwald, J., Hankovszky, H. O., and Hideg, K. (1982) A novel reversible thiol-specific spin label: papain active site labeling and inhibition. *Anal. Biochem.* 119, 450–455.
- (58) Camilloni, C., and Vendruscolo, M. (2013) A relationship between the aggregation rates of  $\alpha$ -synuclein variants and the  $\beta$ -sheet populations in their monomeric forms. *J. Phys. Chem. B* 117, 10737–10741.
- (59) Knowles, T. P., Waudby, C. A., Devlin, G. L., Cohen, S. I., Aguzzi, A., Vendruscolo, M., Terentjev, E. M., Welland, M. E., and Dobson, C. M. (2009) An analytical solution to the kinetics of breakable filament assembly. *Science* 326, 1533–1537.
- (60) Jha, A. K., Colubri, A., Freed, K. F., and Sosnick, T. R. (2005) Statistical coil model of the unfolded state: resolving the reconciliation problem. *Proc. Natl. Acad. Sci. U. S. A.* 102, 13099–13104.
- (61) Hus, J.-C., and Brüschweiler, R. (2002) Principal component method for assessing structural heterogeneity across multiple alignment media. *J. Biomol. NMR* 24, 123–132.
- (62) Hansen, M. R., Hanson, P., and Pardi, A. (2000) Filamentous bacteriophage for aligning RNA, DNA, and proteins for measurement of nuclear magnetic resonance dipolar coupling interactions. *Methods Enzymol.* 317, 220.
- (63) Paravastu, A. K., Leapman, R. D., Yau, W.-M., and Tycko, R. (2008) Molecular structural basis for polymorphism in Alzheimer's  $\beta$ -amyloid fibrils. *Proc. Natl. Acad. Sci. U. S. A.* 105, 18349–18354.